ADVANCED FUNCTIONAL MATERIALS

www.afm-journal.de

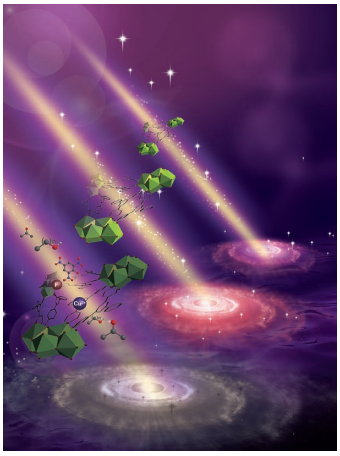

Sensors

A red-emitting Eu metal–organic framework (EuMOF) is successfully obtained by S.-Y. Song, H.-J. Zhang, and co-workers and serves as a multi-responsive luminescent sensor toward different organic molecules and inorganic ions. On page 4034, the red emission signal is changed after exposing the EuMOF to the analytes under UV light excitation: some of them even quench the luminescence. This work paves the way for the practical application of luminescent MOF sensors for pollutant detection.

Solar Cells

Nanohybrid heterojunction (NH-HJ) solar cells are developed on page 4042 by M. A. El Khakani and co-workers using pulsed laser deposition (PLD) to decorate TiO_2 nanorods and single carbon nanotubes with PbS nanoparticles, and to integrate the formed nanohybrids directly into photovoltaic devices. This approach offers the latitude to achieve the direct assembly of different nanomaterials, thereby forming novel nanohybrids. By optimizing the size of the particles and tube lengths, NH-HJ solar cells exhibiting power conversion efficiencies as high as 5.3% are achieved.

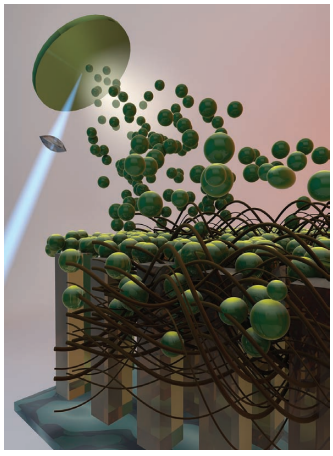

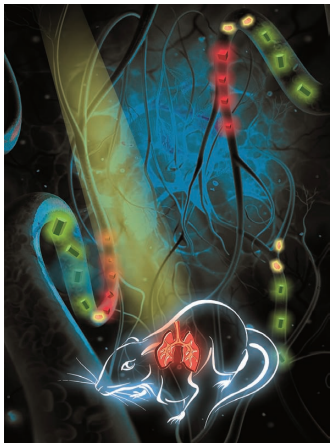

Upconversion

On page 4051, S. J. Zeng, H. R. Liu, J. H. Hao, and co-workers report an Mn^{2+} doping strategy for a new type of multifunctional upconversion nanoprobe based on a $NaLnF_4$:Yb/Er system with controlled phase/size, tunable multi-color output, and dominant red upconversion emission. The nanoprobe can be used for multi-modal upconversion luminescence and X-ray bioimaging with deep tissue penetration. Most importantly, the blood vessels of the lung can be visualized, which promises faster and more accurate prognosis of pulmonary vascular diseases.

FULL PAPERS

Drug Delivery

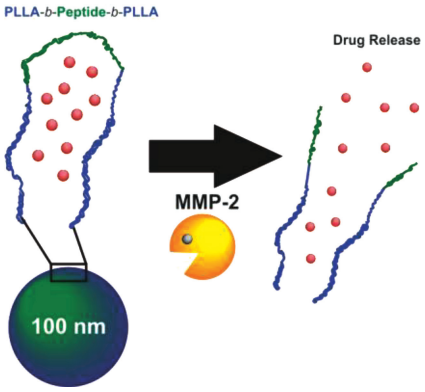

Triblock copolymer nanoparticle with tunable drug release. Nanocarriers based on PLLA-*b*-peptide-*b*-PLLA copolymers are proved to have exceptional material properties for controlled drug release in response to MMP-2-dependent peptide cleavage. Comparison specimens demonstrate the tunable bioactivity of these nanocarriers based on polymer constitution. As MMP-2 is selectively overexpressed in tumor tissues, this is a promising system for solid tumor cancer therapy.

Sensors

Multi-responsive fluorescent sensing is achieved using a Eu metal–organic framework (EuMOF). Accessible Lewis-base sites and coordinated water molecules are successfully anchored on the EuMOF-based sensor for the recognition of different analytes at the molecular level. This strategy paves the way for the practical application of luminescent MOF sensors in pollutant-detection.

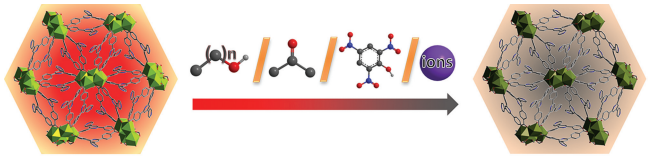

Solar Cells

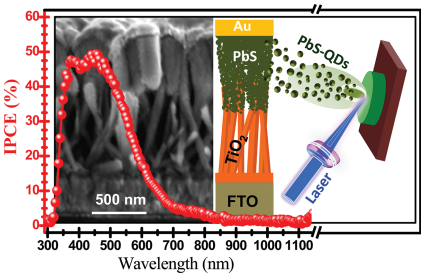

Pulsed laser deposition (PLD) is advantageously used to decorate TiO_2-nano rods (TiO_2-NRs) with PbS-quantum dots (PbS-QDs) to achieve highly efficient nanohybrid-heterojunctions (NH-HJ) solar cells. By optimizing the characteristics of both PLD-deposited PbS-QDs and TiO_2-NRs, while introducing MoO_3 hole extracting layer and single-wall carbon nanotubes efficient charge carrier, NH-HJ PV-devices exhibit power conversion efficiencies as high as 5.3% (under AM1.5 solar illumination).

Upconversion

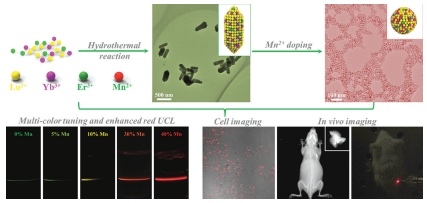

A transition metal Mn^{2+} doping method for the simultaneous phase/size control, multicolor output from green to red, and remarkably enhanced red emissions in $NaLnF_4$ upconverting nanoparticles (UCNPs) is demonstrated. In vivo UC and X-ray bioimaging reveal that these UCNPs are ideal probes for in vivo multimodal bioimaging with high contrast, deeper tissue penetration, and improved detection of pulmonary vascular diseases.

FULL PAPERS

Composite living fibers (CLFs) are fabricated to create tissue constructs using weaving, knitting, braiding, winding, and embroidering. The CLFs are formed from a core load-bearing synthetic polymer and one or multiple layers of cell- or drug-loaded hydrogels. This strategy lays the foundation for engineering complex 3D tissue-like constructs by using textile processes.

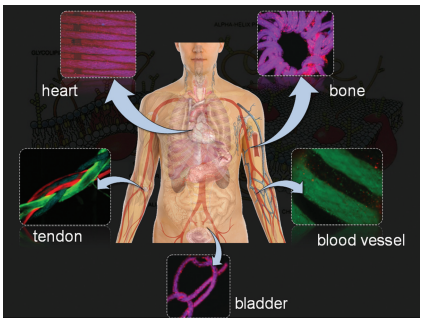

Tissue Engineering

Splitting excitons into free charges can be very efficient at polymer/fullerene interfaces but it becomes a challenging task when the fullerene is replaced by a polymeric acceptor. Here, the structural origin of the photocurrent generation in P3HT:P(NDI2OD-T2) all-polymer solar cells is investigated. A proper relative orientation of the polymer crystallites is needed to create free charge carriers.

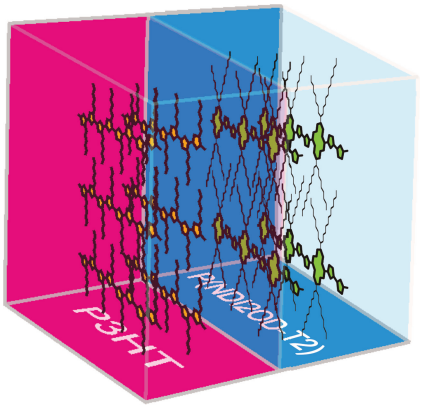

Solar Cells

Selenium sulfide/carbonized polyacrylonitrile composites (SeS_x/CPAN) are synthesized by annealing a mixture of SeS_2 and polyacrylonitrile at 600 °C under vacuum. SeS_x/CPAN composites exhibit a high specific capacity, long cycle life, and superior rate capability. At a current density of 600 mA g^{-1}, it maintains a reversible capacity of 780 mAh g^{-1} for 1200 cycles.

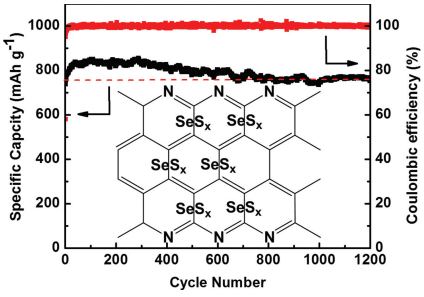

Cathodes

A 3D stack integrated TENG is rationally designed to harvest ambient vibration energy. With superior operation synchronization, the 3D-TENG produces a remarkable peak power density of 104.6 Wm^{-2}. The capability of harvesting kinetic energy when people play various kinds of ball sports is demonstrated. And large amount of these self-powered balls can also be woven into webs for ocean wave energy harvesting, which can be potentially applied to large-scale energy generation.

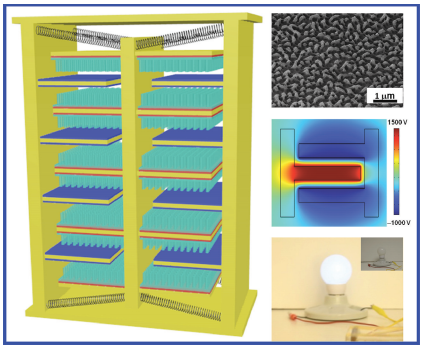

Energy Harvesting

CONTENTS

FULL PAPERS

Anode Materials

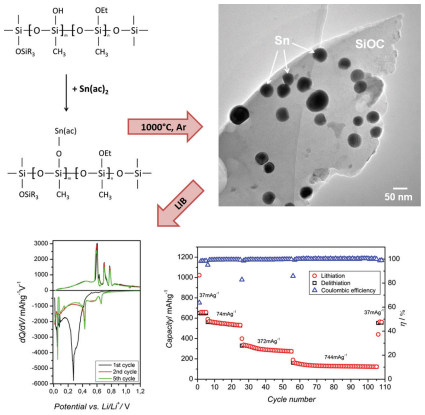

Enhanced lithium storage stability of single-source precursor-derived SiOC/Sn nanocomposites is demonstrated. The nanocomposites comprise an amorphous SiOC matrix and in-situ formed Sn precipitates. Capacity measurements outline different final Li–Sn alloy stages, depending on the matrix. Galvanostatic cycling shows a first cycle reversible capacity of 566 $mAhg^{-1}$ for SiOCMK/Sn and 651 $mAhg^{-1}$ for SiOCRD/Sn.

Solar Energy

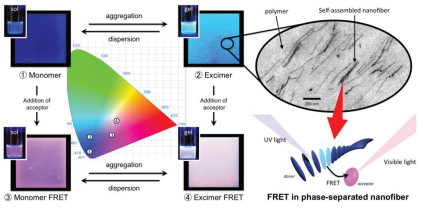

A new strategy for spectral conversion through efficient energy transfer in a phase-separated nano-sized domain is demonstrated. This approach can be defined as utilization of a highly oriented nano-sized phase separation in a polymer matrix using a self-assembling technique. The power-conversion efficiency of a CIGS solar cell is improved by addition of an spectral conversion coating.

Resistive Switching

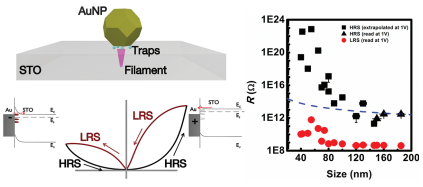

Size dependent resistive switching is demonstrated across nanoscale metal-$SrTiO_3$ interfaces ranging from 20 to 200 nm. The size dependent resistance of the high resistance state results from changes in both the interfacial area and Schottky barrier. The low resistant state exhibits size independent resistances due to the dominant fast conductive path induced by electroforming.

Stimuli-Responsive Polymers

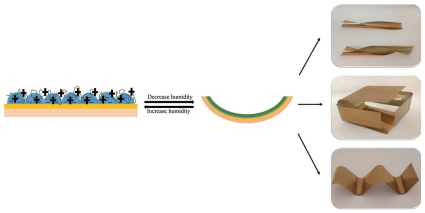

Self-folding polymer-based materials are fabricated by depositing a humidity responsive polymer layer on plastic substrates of various dimensions. A mathematical model is developed to describe and predict the self-folding characteristics of these devices. Using this model, it is possible to design materials that self-fold into predetermined three-dimensional structures of varying complexities.

FULL PAPERS

Single-wall boron nanotubes are shown to be stable at the experimentally reported synthesis temperature of 870 °C by first-principles molecular dynamics simulations. The atomic structure of the nanotube's walls consist of different mixed triangular–hexagonal structural motives. This substantiates the importance of mixed triangular–hexagonal morphologies as a structural paradigm for atomically thin boron.

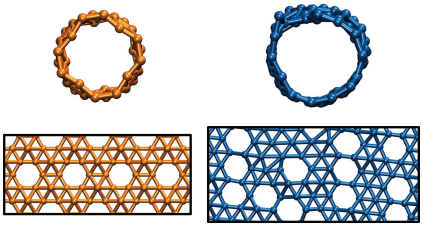

Boron

Programmable polymer composite platforms provide a means for the design and fabrication of transient electronic devices and bioelectronics with precise control over transiency rate. The chemical composition of biocompatible and biodegradable polymer films is manipulated to achieve desired mechanical properties and solubility rates for specific applications ranging from transient electronics to bioelectronics.

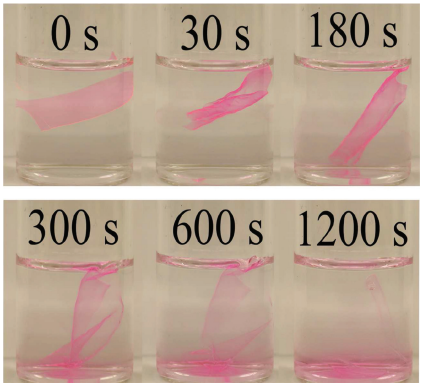

Controlled Degradation

Core–shell photoresponsive protein–graphene–protein capsules supported on a reduced graphene oxide substrate and one-single component of protein display targeted chemotherapy with synergistic hyperthermia effects, eradicating not only the targeted cells but also cancerous cells omitted near infrared irradiation in vivo and in vitro.

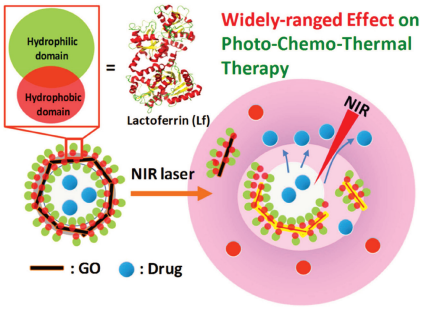

Nanocapsules

A rational design of Cu-stablized S-microporous carbon composite cathodes for Li–S batteries is presented in this study. By the combination of physical restriction for S/polysulfids from MC and chemical restriction from nano-Cu, the MC-Cu-S cathode with high S loading shows excellent electrochemical performance in low-cost carbonate solvent-based electrolyte.

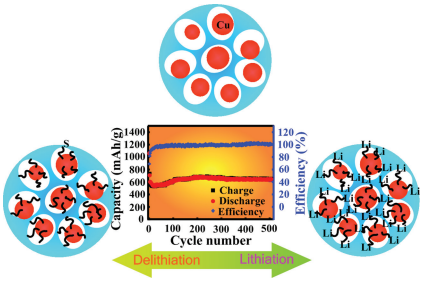

Energy Storage

CONTENTS

FULL PAPERS

Organic Electronics

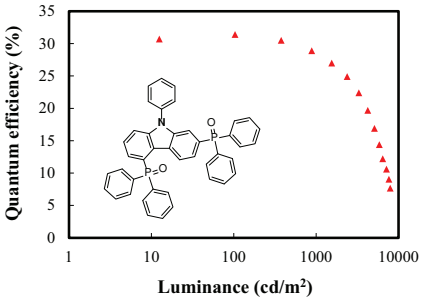

Excellent thermal stability and high quantum efficiency above 30% in blue phosphorescent organic light emitting diodes are achieved using a high triplet energy host material with two electron withdrawing substituents at asymmetric positions of carbazole.

Semiconductors

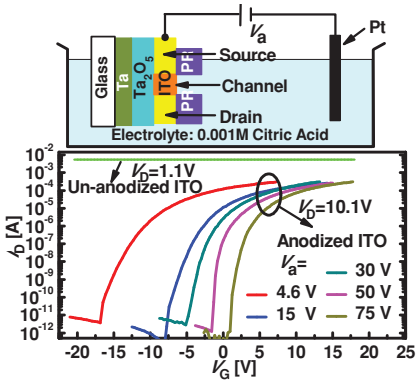

Electrical, optical, and structural properties of ITO film are significantly modulated by an anodization process. The anodized ITO TFT technology results in an ideal homo-junction structure with source/drain/pixel electrodes and channel region all made of one single ITO layer. The room temperature fabricated TFT shows an on/off ratio over 10^8, a mobility of 29.0 $cm^2\ V^{-1}\ s^{-1}$ and sub-threshold swing of 0.20 V per decade. This technology also allows a feasible V_T adjustment and muti-V_T implementation.

Anode Materials

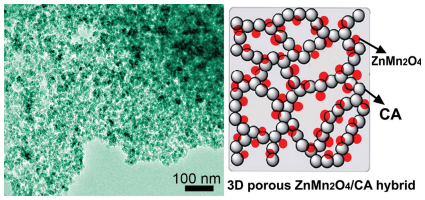

Based on the advantages of high surface area, abundant porosity, the good electron transport properties of carbon aerogel (CA) materials, and the good electrochemical properties of nanostructured spinel $ZnMn_2O_4$ oxide materials, these 3D interconnected spinel $ZnMn_2O_4$/CA hybrids display a significantly improved electrochemical performance with a high reversible specific capacity, specific capacity, and rate capability, as well as excellent cycling performance.

Energy Storage

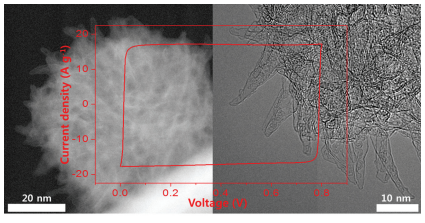

A hierarchical design and a cost-effective approach to fabricate high performance supercapacitors using high charge density carbon nano-particles (HCDN) are reported. A special arc synthesis method is used to synthesized B, N co-doped HCDN. Subsequent hierarchical optimization and integration processes result in high performance supercapacitor exhibiting very high power density (4.58 $kW\ cm^{-3}$) and energy density (2.45 $mWh\ cm^{-3}$).